J. Fluid Mech. (1992), *vol.* 241, *pp.* 233–260
Printed in Great Britain

Numerical experiments on two-dimensional foam

By THOMAS HERDTLE AND HASSAN AREF
Department of Applied Mechanics and Engineering Science, University of California at San Diego, La Jolla, CA 92093-0411, USA

(Received 26 August 1991 and in revised form 23 January 1992)

The statistical evolution of a two-dimensional polygonal, or 'dry', foam during diffusion of gas between bubbles lends itself to a very simple mathematical description by combining physical principles discovered by Young, Laplace, Plateau, and von Neumann over a period of a century and a half. Following a brief review of this 'canonical' theory, we report results of the largest numerical simulations of this system undertaken to date. In particular, we discuss the existence and properties of a scaling regime, conjectured on the basis of laboratory experiments on larger systems than ours by Glazier and coworkers, and corroborated in computations on smaller systems by Weaire and collaborators. While we find qualitative agreement with these earlier investigations, our results differ on important, quantitative details, and we find that the evolution of the foam, and the emergence of scaling, is very sensitive to correlations in the initial data. The largest computations we have performed follow the relaxation of a system with 1024 bubbles to one with $O(10)$, and took about 30 hours of CPU time on a Cray-YMP supercomputer. The code used has been thoroughly tested, both by comparison with a set of essentially analytic results on the rheology of a monodisperse-hexagonal foam due to Kraynik & Hansen, and by verification of certain analytical solutions to the evolution equations that we found for a family of 'fractal foams'.

1. Introduction

The coarsening of a foam due to diffusion of gas from small bubbles, where the pressure is large, to large bubbles, accompanied by the intermittent disappearance of small bubbles, and the reconnection of soap films within the foam, is a fascinating dynamical process. In two dimensions the formation of ever larger bubbles reminds one of the 'inverse' cascade in two-dimensional turbulence, that has been the object of considerable study.

It is at first sight surprising that the evolution of a two-dimensional 'dry' foam can be completely expressed in terms of the vertices of the bubbles and their pressures, so that a fully deterministic, finite system of evolutionary equations results. The ingredients in this description are: (i) the Young–Laplace law, formulated in 1805–6, for the pressure difference across a two-fluid interface with surface tension; (ii) Plateau's (1873) rule that films in the foam meet three at a time at angles of 120°; and (iii) von Neumann's (1952) law that the rate of change of area of an n-sided bubble due to gaseous diffusion is proportional to $n-6$. The fusion of these three physical principles makes up what we call the 'canonical' model of two-dimensional foam evolution. We explain the physics of this model in more detail in §2.

This paper reports numerical experiments using our implementation of the canonical model in a computer code. Numerical considerations, and details of the

implementation, which differs from the pioneering work of Weaire & Kermode (1983*a*, *b*; 1984; see also Kermode & Weaire 1990), are the subject of §3. Our code treats, we believe for the first time, the fully coupled system of bubbles in the foam, and thus captures certain long-range correlations that appear to be significant for the statistics. We have found that rather large computations are required to capture statistical scaling behaviour in this system. Such computations are quite time-consuming. The relaxation of some 1000 bubbles in the initial state to a few in the final state required on the order of 30 CPU hours on a single processor of a Cray-YMP8/864 supercomputer. The computer time per step was optimized to be $O(N^{1.3})$, where N is the number of bubbles. Preliminary results on smaller systems (using a less efficient code) were reported by Herdtle & Aref (1989) and Aref & Herdtle (1990). The latter paper reviews numerous 'topological' properties of two-dimensional foam, that we shall use here on several occasions without further development.

Before embarking on large simulations, it is essential to verify the code constructed on a number of smaller test calculations where analytical answers are known. We have conducted two main tests of this kind. In one series of computations we reproduced the rheological properties found by Kraynik & Hansen (1986) for a monodisperse-hexagonal foam. In a second development we found a family of analytical solutions for the relaxation of 'fractal foam', decorating a vertex between larger bubbles, and we verified that these solutions are tracked by our code to machine precision. The analysis of the fractal foams has been published separately (Herdtle & Aref 1991*a*). We discuss code verification in §4.

In §5 we report our simulation results for large systems. We have conducted several numerical experiments starting from 1024 bubbles. The initial states were obtained using the Voronoi construction, as has become rather standard in simulations of this kind (see §3.3). Simple topological considerations show that the average number of sides per bubble is $\langle n \rangle = 6$. Hence, the lowest-order moment of $\rho(n)$, the number-of-sides frequency distribution, that is useful for differentiating bubble patterns is the second moment

$$\mu_2 = \langle (n-6)^2 \rangle. \tag{1.1}$$

We present results for several initial values of this parameter, as has been done recently also by Weaire & Lei (1990).

The main result to be found in the literature on statistical evolution of two-dimensional foam, coming both from laboratory experiments on large systems with up to 10000 bubbles by Glazier, Gross & Stavans (1987; see also Glazier 1989; for a popular account see Maddox 1989), and from numerical simulations of much smaller systems (Weaire & Lei 1990), is the emergence of a scaling state with a value of $\mu_2 = 1.42 \pm 0.05$. The corresponding scaling form of the distribution $\rho(n)$ in experiments has a slightly *higher* value of $\rho(5)$ than $\rho(6)$. Another scaling result is the existence of a power-law regime for the number of bubbles versus time, $N \propto t^{-\alpha}$, where values of $\alpha \approx 0.6$ are given from experiment. Recent experiments by Stavans (1990), where a better approximation to the 'dry' foam limit that is used in the simulations is achieved by continually draining the foam, report scaling values of $\alpha \approx 1.0$.

We have monitored the above scaling predictions in our simulations, along with a host of other statistical diagnostics. We find values of $\mu_2 \approx 1.2$ for the scaling regime, a scaling function $\rho(n)$ that peaks at $n = 6$, and a steep power-law decay for the number of bubbles with time corresponding to $\alpha \approx 1.0$–1.2. We find that there can

be very long transients so that for some initial states the system never really settles down to a scaling state.

We have also performed a large simulation starting from an initial condition that is unstressed to assess any influence this might have on the results. (All previous simulations have had some net stress along the periodic boundaries.) We have performed a simulation for a foam contained within a rigid, circular container to see if the boundary conditions have an effect on statistics, since they do, clearly, have an effect on asymptotic states (Aref & Herdtle 1990). This simulation is also of interest to the experimental situation where any effect of bounded containers cannot easily be eliminated. Realizing that the effect of initial conditions can be extremely long-lived, we have also artificially suppressed the number of hexagons in the initial state to remove any bias towards hexagons, which appear as the most favoured shape later on. We found that the distribution $\rho(n)$ at large times returned to an equilibrium with $\rho(6) > \rho(5)$. All these results are discussed in §5.

There are several reasons one can list that a laboratory experiment in a shallow container with rigid boundaries might deviate from the canonical model, and inconsistencies between experimental measurements and dry foam simulations are to be expected. The disagreement with earlier numerical simulations, allegedly solving the same system of equations, is more troubling. However, the differences in implementation between our work and the earlier work (Weaire & Kermode 1983*a*, *b*; 1984; Kermode & Weaire 1990) are non-negligible. We revisit them in our final §6, where the main results obtained are summarized and discussed, conclusions are drawn, and various possible extensions of the work are commented upon.

2. Physics of two-dimensional 'dry' foam: the canonical model

The nature of the real-space structure being considered is a tiling of the plane (Grünbaum & Shephard 1987) by polygonal tiles with sides that are circular arcs. This comes about because of the Young–Laplace law, which states that the pressure difference, Δp, across a film is

$$\Delta p = 2\sigma\left(\frac{1}{R_1}+\frac{1}{R_2}\right). \tag{2.1}$$

Here σ is the surface tension coefficient, and R_1 and R_2 are the principal radii of curvature of the surface. It is assumed that σ is constant throughout the foam, and constant in time. The factor of two arises because there are two liquid–gas surfaces to the film. In two dimensions, of course, one of the radii of curvature is infinite, and (2.1) implies that each film is a circular arc. This is a tremendous simplification! It is possible to have foams in three dimension where each surface is a portion of a sphere (cf. Herdtle & Aref 1991*b*; Sullivan 1991) but in general this may not even be a good approximation.

The tiling provided by a two-dimensional foam is *tri-valent* (in the terminology of Grünbaum & Shephard 1987) according to Plateau's (1873) rule that three films must meet in an edge. (In two dimensions the edges are the vertices of the foam.) Since the three angles must all equal 120°, the tiling is also *monogonal* in Grünbaum & Shephard's (1987) classification. Physically, the equality of the three angles at each vertex of the two-dimensional tiling is due to the elastic forces within the soap films. It is assumed that the elastic relaxation to 120° angles is so rapid compared to the process of gas diffusion between bubbles that we may treat it as instantaneous.

It is also appropriate to comment on the use of the word 'dry'. In a real foam some

liquid will collect at the vertices, i.e. within the edges at which the films meet. This liquid forms what are called *Plateau borders* or *Gibbs rings* (cf. Isenberg 1978). The amount of liquid available for these borders depends on the total amount of liquid left in the foam. In the model discussed here the Plateau borders are assumed to be so small that we may ignore them. This is the limit of a 'dry' foam to which the 'canonical' model pertains. Recently, attempts have been made to include the Plateau borders by 'decorating' the vertices in a dry foam with pockets of liquid (Bolton & Weaire 1991). Plateau borders complicate the problem considerably, and we have not attempted to include them in our description.

The final ingredient required for the canonical model is a 'rule', first noticed by von Neumann (1952), which states that the rate of change of area of an n-sided bubble in a two-dimensional foam is proportional to $n-6$. The physical basis for this rule is that gas diffuses from bubble to bubble with a flow rate through any given soap film that is proportional to the pressure difference across that film (see, for example, the discussion by Princen & Mason 1965). The total flux of gas from one bubble to a neighbouring bubble is proportional to the pressure difference times the length of the common film. This length can be written as the radius of the arc in question times the opening angle. Since the pressure difference is inversely proportional to the radius by the Young–Laplace law, the gas flux across a film ends up being proportional simply to the opening angle of the film arc. Summing these angles over the closed polygonal bubble, and recalling that the angles between arcs at each vertex are 120°, immediately gives the result

$$\frac{\mathrm{d}A_n}{\mathrm{d}t} = \frac{\pi}{3}\kappa\sigma(n-6), \tag{2.2}$$

where κ is a constant proportional to the permeability of the soap films (again assumed to be the same throughout the foam, and constant in time).

In Aref & Herdtle (1990) we also discussed the modification of (2.2) that occurs for bubbles adjacent to a rigid boundary. A simple extension of the arguments above, noting that no gas can escape through the side made up of a rigid boundary, gives the result

$$\frac{\mathrm{d}A_n}{\mathrm{d}t} = \kappa\sigma\left\{\frac{\pi}{3}(n-5)+\theta\right\} \tag{2.3}$$

for bubbles on the boundary. Here θ is the angle (in radians) through which the tangent to the boundary has turned from one point of contact between bubble film and rigid surface to the other. The rigid boundary is assumed to be wetted by soap film so that bubble sides come into it at 90° angles. Equations (2.2)–(2.3) as written are consistent in the sense that (2.2) pertains to bubbles in the interior of a bounded foam, while (2.3) governs the evolution of bubbles on the boundary.

The physical picture developed so far allows us to write evolution equations for the two-dimensional foam. Our basic degrees of freedom are the two coordinates of each vertex in the foam, and the pressures of all the bubbles. Since the pressure differences between bubbles give us the radii of the sides, we can use elementary plane geometry to write formulae for the areas of all bubbles in terms of the variables given. There is one indeterminacy here. Given two points and a radius, there are really two circular arcs with the given radius that will pass through the two points. These two arcs are illustrated in figure 1. We consistently choose the 'shorter' of the two arcs on the basis that the foam will seek to minimize the total film length (and on the basis of experimental observations).

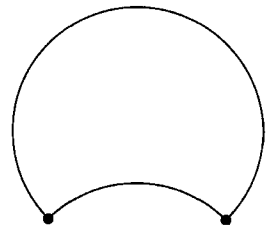

FIGURE 1. Illustrating the two possible arcs of a given radius passing through two given points. The shorter of the two arcs is chosen as the film configuration in a doubly periodic foam for a given pressure difference.

We may also write formulae for the angles formed between films at a vertex. We know that these angles should be 120°, but consider the formulae to have been written for the general case. In summary, we have a set of expressions for areas and angles at vertices in terms of vertex coordinates and bubble pressures. We choose two angles at each vertex, since the third angle is obtained by subtracting the sum of the chosen two from 360°. We see that the number of dependent variables, one area per bubble and two angles per vertex, are equal in number to the independent variables, one pressure per bubble and two coordinates per vertex.

Collect the independent variables into a vector

$$\boldsymbol{X} = (p_1, \ldots, p_F, x_1, y_1, \ldots, x_V, y_V), \tag{2.4}$$

where V is the number of vertices, and F the number of 'faces' or bubbles in the foam. The x and y are coordinates in an arbitrarily chosen frame of reference relative to which the foam as a whole is stationary. The p are the bubble pressures.

Similarly, collect the set of areas and angles into a vector

$$\boldsymbol{Y} = (A_1, \ldots, A_F, \Theta_1, \Phi_1, \ldots, \Theta_V, \Phi_V). \tag{2.5}$$

Some convention must be introduced to select just two angles, Θ_i and Φ_i, at vertex i. The A denote the areas of the bubbles. We argued above that elementary plane geometry yields a functional relationship

$$\boldsymbol{Y} = \mathscr{F}(\boldsymbol{X}). \tag{2.6}$$

Consider now an infinitesimal, 'virtual' rearrangement of the foam wherein $\boldsymbol{X}$ changes by $\mathrm{d}\boldsymbol{X}$, and $\boldsymbol{Y}$ consequently changes by $\mathrm{d}\boldsymbol{Y}$. The Jacobian, $\boldsymbol{J}$, of the transformation from $\boldsymbol{X}$ to $\boldsymbol{Y}$ in (2.6) relates the two:

$$\mathrm{d}\boldsymbol{Y} = \boldsymbol{J}\mathrm{d}\boldsymbol{X}; \quad \boldsymbol{J} = \frac{\partial \mathscr{F}}{\partial \boldsymbol{X}}. \tag{2.7}$$

The calculation of the elements of $\boldsymbol{J}$ can be done analytically, since all the formulae summarized as (2.6) are known. The Jacobian is an $(F+2V)\times(F+2V)$ matrix. For periodic boundary conditions $V = 2F$ by Euler's polyhedral formula (cf. Aref & Herdtle 1990). Hence, $\boldsymbol{J}$ is a $5F \times 5F$ matrix. However, it is very sparse. For example, for 100 bubbles, $\boldsymbol{J}$ has 500×500 entries. The last 400 rows will each have exactly 9 non-zero entries, since each angle depends only on the coordinates of the vertex at its apex, the coordinates of the two vertices forming its legs, and the three pressures in the bubbles around its apex, making a total of 9. The first 100 rows will have 19

non-zero entries per row, on average, since each cell has 6 neighbours on average, and the area of a cell depends on its own pressure and the pressures in its neighbouring cells (7 numbers, on average), as well as on the coordinates of its vertices (12 numbers, on average). Figure 2 shows the pattern of entries in $\boldsymbol{J}$ that are non-zero for a foam with 100 bubbles, and the numbering of vertices and bubbles that we actually used in the computations. This figure pertains to the initial state of the foam set by the Voronoi construction (§3.3). The sharp, curved boundary, at the top and side of figure 2, which reflects the numbering of vertices and bubbles, is gradually broken as reconnections in the foam take place. The reader is invited to verify the counting of 9 and 19 non-zero entries mentioned above. Although sparse, this diagram of non-zero elements of $\boldsymbol{J}$ shows that the foam is a many-body problem capable of sustaining long-range correlations.

The Jacobian $\boldsymbol{J}$ is singular, since a rigid translation of the entire foam relative to the periodic box will have no effect on angles and areas. Hence, if $\mathrm{d}\boldsymbol{X}$ is chosen to correspond to such a translation, the corresponding vector $\mathrm{d}\boldsymbol{Y}$ vanishes. The same is true if $\mathrm{d}\boldsymbol{X}$ corresponds to a uniform addition of pressure to all bubbles (unless there is some boundary condition on the pressure), since only pressure differences effect changes in the geometry.

It appears (from numerical computations) that the null space of $\boldsymbol{J}$ is limited to those $\mathrm{d}\boldsymbol{X}$, such as rigid displacements or uniform pressure changes, that one expects on physical grounds. In particular, the null space is small. With the understanding that the null space is dealt with separately, we consider the formal inversion of (2.7),

$$\mathrm{d}\boldsymbol{X} = \boldsymbol{J}^{-1}\,\mathrm{d}\boldsymbol{Y}. \tag{2.8}$$

We may distinguish two types of processes (which become the possible 'steps' in the numerical implementation below): (i) *elastic relaxation*, in which the areas of individual bubbles do not change, and the angles all adjust to 120°; and (ii) *diffusion*, in which the areas change according to von Neumann's law, (2.2), but the angles remain fixed. The evolution of the foam may be considered to be a succession of steps of type (ii), with steps of type (i) as useful tools for initialization (e.g. from a Voronoi construction, where the angles are not 120°; see §3.3), as an occasional 'control', and, as we shall see below, as an essential ingredient following a topology change in the foam.

The above considerations allow us, in principle, to evolve the foam due to diffusion. We shall comment on how this is actually done in the next section. Here we must address the important augmentation of the framework established so far that is required whenever a film in the foam approaches zero length. Figure 3 shows examples of how this can happen. Two basic processes are at work. In the T2 change a three-sided bubble contracts to a point. In the T1 change a single film contracts to zero length, and a reconnection takes place in which the two adjoining bubbles each lose a side, with two other neighbouring bubbles each gaining a side. Both these processes change the association of vertices, areas, and angles with bubbles that is implicit in (2.4), (2.5). Indeed, a T2 process eliminates one pressure and two vertices from $\boldsymbol{X}$.

The new topology and reassignment of vertices to bubbles is enforced whenever the simple evolution (2.8) produces a side of length zero. This type of singularity happens readily and frequently. It is a change in the topology of the system akin to the merging of two vortices in two-dimensional turbulence. Physically, the process of reconnection is rapid compared to diffusion. The evolution of the foam may be thought of as the slow diffusion of gas between bubbles interrupted suddenly and

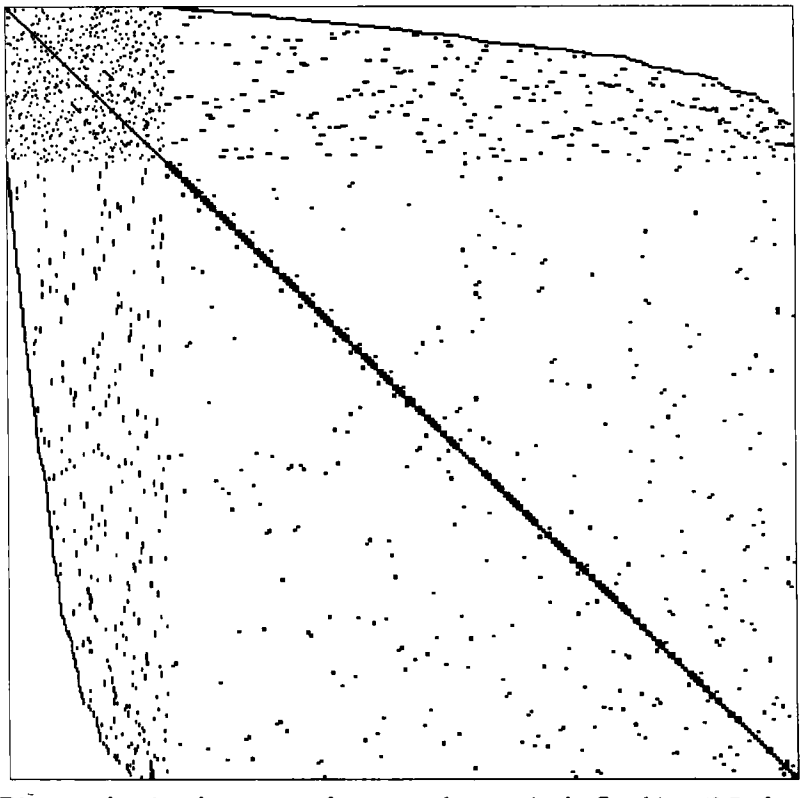

FIGURE 2. Diagram showing the pattern of non-zero elements in the Jacobian, (2.7), for a foam with 100 bubbles and the convention for numbering of vertices and bubbles that was actually used computationally.

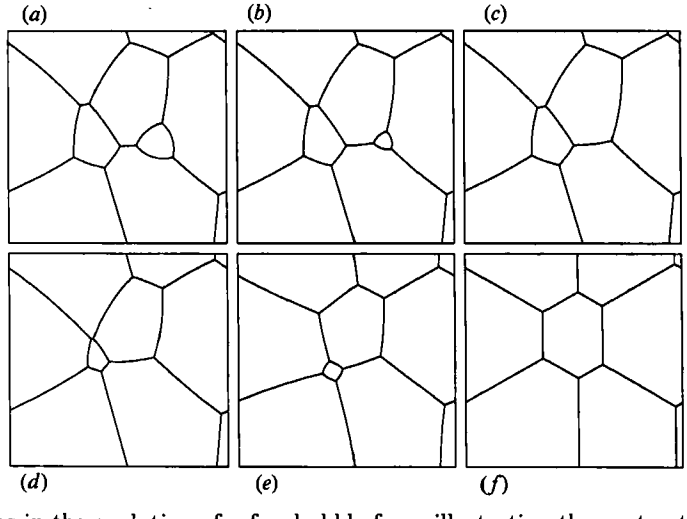

FIGURE 3. Stages in the evolution of a few-bubble foam illustrating the contraction to a point of a three-sided bubble (T2 change; (*b*) to (*c*)). Also shown is the reconnection (T1 change) due to the vanishing of a film separating a five-sided from a seven-sided bubble (*d*, *e*). The resulting four-sided bubble disappears (*e*, *f*) due to a T1 immediately followed by a T2.

intermittently by topology changes. The adjective 'punctuated' has been used for dynamics of this kind. Elastic relaxation steps, type (i) above, are essential in bringing a newly reconnected configuration back to a state of mechanical equilibrium.

3. Computer implementation

The various steps and procedures described in the preceding section lead to several interesting numerical analysis problems when implementation in a computer code is considered. As we describe our solutions to these we shall frequently refer to the pioneering computational work aimed at solving the canonical model by Weaire & Kermode (1983*a*, *b*; 1984). We shall ignore for the present the hexagonal lattice model pursued by Wejchert, Weaire & Kermode (1986), which, however promising, has yet to yield results of comparable resolution to a continuous space approach, such as we use here. We also ignore phenomenological models, such as that of Beenakker (1988), since they do not represent discretizations of the full equations of the canonical model described in §2. The most comprehensive description of the prior methodology appears in Kermode & Weaire (1990, abbreviated as KW in what follows).

3.1. *Differences with the computer code of Kermode & Weaire*

The first main difference between our code and KW is that in any time step we tackle the full system (2.7) or (2.8) at once, whereas KW partition it into a sequence of 5×5, uncoupled subsets involving the degrees of freedom $\mathrm{d}x$, $\mathrm{d}y$, $\mathrm{d}p_1$, $\mathrm{d}p_2$, $\mathrm{d}p_3$, where $(\mathrm{d}x, \mathrm{d}y)$ are the changes in the coordinates of a vertex in the foam, and $\mathrm{d}p_1$, $\mathrm{d}p_2$, $\mathrm{d}p_3$ are the pressure changes in the three bubbles sharing that vertex. In the method of KW: 'Each iterative step consists of a change of the coordinates of one vertex and the pressures of the three neighbouring cells... Each vertex is treated in turn, and the entire cycle repeated (typically ten times) to achieve convergence. The local relaxation is designed to take the structure towards fulfilment of the equilibrium conditions for given cell areas...'. Of course, iterating these submatrix calculations to convergence over the entire foam is, in principle, equivalent to solving the full system at once as we do (although it may be a less efficient way of solving a sparse matrix equation). However, reconnections within the foam during these iterations should not be allowed.

The second main difference between our implementation and KW is that the entries in the matrix $\boldsymbol{J}$ are calculated analytically for our case, whereas in KW the corresponding derivatives in the 5×5 submatrix are computed numerically using one of 'two methods supplied, namely the standard "slope" calculation and Richardson's extrapolation... The choice of method used is defined by the user...'

The third main difference with KW is in the criterion used for effecting a reconnection. With reference to figure 4(*a*), where $\boldsymbol{x}_i = (x_i, y_i), \boldsymbol{x}_j = (x_j, y_j)$ are the present positions of two neighbouring vertices, and $\mathrm{d}\boldsymbol{x}_i$ is the change in position of vertex i, computed by the 5×5 subsystem described above, KW perform a T1 change if

$$|\boldsymbol{x}_i - \boldsymbol{x}_j|^2 < (\boldsymbol{x}_j - \boldsymbol{x}_i) \cdot \mathrm{d}\boldsymbol{x}_i. \tag{3.1}$$

We re-emphasize that implementing a T1 change while the submatrix solutions are being iterated to produce a pure diffusion step can lead to spurious T1 changes. Only after all vertices have been adjusted in a diffusion step can the configuration be assessed for potential topology changes. We do not see (3.1) as a terribly convincing criterion in that context.

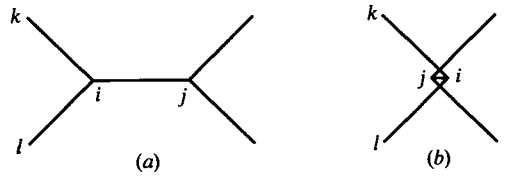

FIGURE 4. (*a*) Subset of the foam that may lead to a T1 change if vertices i and j approach. (*b*) Possible crossover that must be detected and addressed by the code. Note that the vertices, j, k, and l, that are neighbours of i, appear in counter-clockwise order in (*a*), but not in (*b*).

By contrast, after a successful diffusion step, our code checks explicitly for the distances to all neighbours of a given vertex, and if a distance falls below a preset cut-off (some small fraction of the box size), a T1 change is effected. After reconnection an elastic relaxation step is performed, and if further edges are found to fall below the cut-off, additional T1 changes are carried out. While this method may appear so straightforward as to be entirely trouble-free, there is one subtlety. It is possible that as the time evolution in (2.7)–(2.8) unfolds, two vertices would cross over as stylized in figure 4(*b*). Thus, just checking the magnitude of distances between vertices does not suffice as a criterion. One must also detect crossovers. Naturally, if a crossover is detected, the step that led to it needs to be reduced so that it does not happen.

To detect crossovers we decide at the outset to keep the vertex connections to neighbours in a counter-clockwise order. The states before and after crossover will now differ in the order in which the neighbouring vertices to vertex i appear: jkl in figure 4(*a*), kjl in figure 4(*b*). The different possibilities are distinguished by the signs of various vector cross-products for vertex separations. Hence, at each time step we compute not only the magnitudes of the vertex separations, but we also check that the appearance of neighbours is still in the correct, counter-clockwise order.

Cell disappearances (T2 changes) are easier to deal with, since they pertain to an area approaching zero. From von Neumann's law one can predict exactly the time when the next three-sided bubble will contract to zero area, and a step of this size can be taken. Our implementation of T2 changes appears to agree with that of KW. We may also comment that whereas KW only adjust time steps to anticipate T2 changes, we adjust time steps to anticipate both T1 and T2 changes. This is discussed in more detail in the following subsection.

It seems clear that the differences between our code and KW can lead to considerable deviations in the results for long-time evolution. Indeed, in §5 we discuss significant differences in the computation of the statistics of large foams relative to earlier work based on the code described in KW. We suspect that the treatment of when and how to initiate a T1 change is the major difference between our implementation of the canonical model and KW, and the main source of disagreement in the results.

3.2. *Additional computational considerations*

The problem of multiple reconnections at a given time arises. In a typical large evolving foam, started from an essentially random initial state, multiple simultaneous reconnections are rare. However, for comparing the code to the results of Kraynik & Hansen (1986), where all reconnections in the monodisperse-hexagonal foam occur at once, it was essential to develop the capability of handling simultaneous reconnections. This is easier to do reliably in a formulation that includes the fully coupled system of equations.

Related to the issue of simultaneous reconnections is the physically relevant issue of topology changes that follow one another very closely in time. For a four-sided cell a T1 change will produce a three-sided cell. Typically, this cell will immediately undergo a T2 change (unless a smaller three-sided cell appears elsewhere in the foam). One can therefore proceed directly to this change before performing the elastic relaxation step.

The solution of (2.8) is the most time-consuming part of the calculations since it involves solving a large linear system. It is essential to take advantage of the sparse nature of the matrix $\boldsymbol{J}$. Addressing this issue has been one of the major improvements in technique since our initial report on foam simulations in Herdtle & Aref (1989) and Aref & Herdtle (1990). Using the least-squares solution routine in the software package SPARSPAK (George & Ng 1984) to solve (2.7) for $\mathrm{d}\boldsymbol{X}$ we have been able to reduce the operation count to $O(N^{1.3})$ per time step. In our earlier work we were using a full singular-value decomposition procedure, resulting in an operation count $O(N^{2.7})$ per time step. This was, however, useful in convincing us that the only null-space vectors $\boldsymbol{X}$ are those that would be anticipated on physical grounds, such as rigid-body translations and uniform pressure changes (as allowed by the boundary conditions). The enhanced efficiency has been a key ingredient in allowing us to perform simulations of the size described in §5. Although these simulations are still quite time-consuming (as mentioned in §1), the memory requirements are small, and we have been able to run at low priority, greatly reducing the actual cost of the calculations. A scalar version of the code has also been running on a Sun SPARCstation for extended periods during the past year. Cross-referencing of results from the two versions of the code running on different computers has been useful on several occasions. We show in figure 5 a plot of the computer time used in one of the large simulations discussed in §5 as a function of the number of bubbles in the foam. The gentle slope reflects the $O(N^{1.3})$ scaling. The intermittent 'bursts' are due to adjustments in step size, producing several small steps, to accurately hit the T1 changes occurring in the foam, followed by the elastic relaxation. The increased computational work takes place at an essentially constant number of bubbles, resulting in the spikes seen in figure 5. (The set of downward spikes in figure 5, much fewer in number, correspond to 'easy' bubble elimination steps, where a T2 change occurs at some vertex with no other changes in foam structure.)

We have so far phrased the evolution of the two-dimensional foam in terms of corresponding infinitesimal changes $\mathrm{d}\boldsymbol{X}$ and $\mathrm{d}\boldsymbol{Y}$, (2.7), (2.8), and, implicitly, correspondingly small steps so that the linearized equations relating these two vectors are accurate. However, from the point of view of computational efficiency there is a clear incentive to make the evolutionary steps as large as possible. Now, during a period where no topology changes take place in the foam, the evolution is really quite simple: the connectivity of films and adjacency of bubbles is fixed, and von Neumann's law (2.2) dictates how much gas is to be transferred into or out of individual bubbles based on their number of sides (and, in particular, *not* their shapes). Hence, an aggressive evolution strategy is to attempt steps that are as large as allowed by the smallest three-sided bubble in the system. Intervening T1 changes will, of course, cut down this step. If the large step is possible, however, the new areas are computed, and an elastic relaxation step is performed to find the new structure. Since the set of areas and angles completely determine the foam structure, use of the linearized approximation (2.7) or (2.8) in determining new positions of the vertices can lead, at worst, to a rigid displacement of the entire foam.

The difficulty in taking large steps is to anticipate any T1 changes so that the code

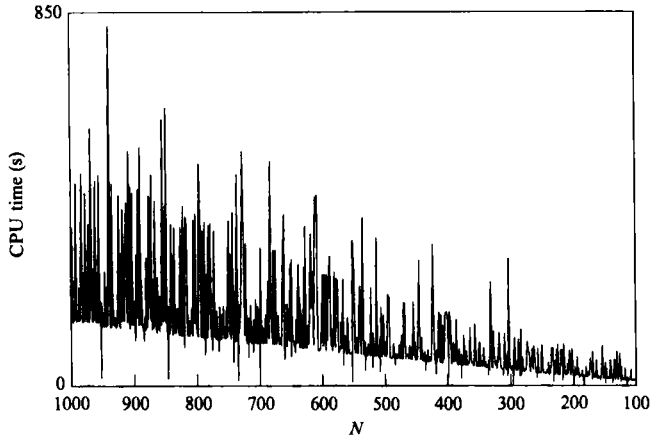

FIGURE 5. Plot of CPU time used (in s) from one bubble disappearance to the next as a function of the number of bubbles. The general decrease due to the $N^{1.3}$ scaling is clearly visible as are the intermittent bursts due to T1 and T2 changes followed by elastic relaxation.

does not overshoot them. (The time for T2 changes can be predicted quite accurately.) We have found that the linear system (2.7) is a useful predictor of when T1 changes will occur, even though it provides only an approximation to the true displacement of vertices for large steps. That is, if a vector $\mathrm{d}\boldsymbol{Y}$ is constructed from von Neumann's law (area changes proportional to time, angle changes zero), and the corresponding vector $\mathrm{d}\boldsymbol{X}$ is computed from (2.8), then $\boldsymbol{X}+\mathrm{d}\boldsymbol{X}$ can be examined for T1 changes (check vertex separations against cut-off, and check for crossovers), and this is a reliable indicator of whether these occur. Since $\mathrm{d}\boldsymbol{X}$ is proportional to time, simple proportionality allows an estimate of when the T1 change will occur, and a large step can be taken (up to some margin of safety). This will reduce the time to the T1 change, and the procedure can be iterated. These acceleration techniques reduce the computer time considerably.

We should stress that the discussion of time steps just given breaks down, in general, when rigid boundaries are present, because the angle θ in the generalized von Neumann's law (2.3), which will be non-zero except for simple geometries with flat boundaries, injects a dependence on the shape of individual bubbles into the diffusion step. Then we have no choice but to continually take small time steps within the confines of the linear approximation (2.7).

As in previous work we do not allow two-sided cells since they would always be unstable. It is believed that the foam could reduce its overall energy if such a cell were to slide to a nearby vertex and become three-sided (Weaire & Kermode 1983*b*). However, a rigorous proof of this appears to be lacking. More appropriate to the simulations is the observation that it would also be impossible to create a two-sided cell during the evolution of the foam. Such a cell could only be created by a T1 change on a three-sided cell, but there is no mechanism to move this hypothetical cell away from the vertex after the T1 change. Thus two-sided cells could only be introduced through the initial conditions, and would quickly disappear by von Neumann's law.

Regarding units, we use the ratio of an area (either the initial, average area per bubble, or the total area of some portion of the foam; the actual choice is specified later as the issue arises) to the coefficient, $\frac{1}{3}\pi\kappa\sigma$, in von Neumann's law as our unit of time. As a unit of length (if needed) we can use the average film length in the foam, or a linear dimension of the domain in question. The average pressure difference,

$\langle \Delta p \rangle$, scaled by σ is a dynamically defined inverse length, that diverges for a polydisperse-hexagonal foam. This discussion of scaling becomes much more interesting for a foam with a compressible gas in the bubbles, a topic that we shall treat elsewhere.

After performing a number of calculations using periodic boundary conditions we decided to produce a video of some of the results. Upon doing this we discovered that the entire foam would shift in an apparently random fashion following a T1 change. The reason for this is that such shifts are null vectors of the Jacobian (2.7), and thus are added in by the SPARSPAK solver. Although such shifts of the foam relative to the periodic boundaries in no way affect the structure, evolution, or statistics of the foam, they are distracting in a video or other continuous graphics.

The physically correct solution to this problem is to keep track of the centre of mass of the foam, and not to allow it to move (since no external force acts on the foam). Although the total area of foam in a doubly periodic box remains unchanged during the evolution, there can be an area flux across the edges. The program needs to keep track of this flux in order to properly track the centre of mass, which must remain fixed during the evolution. When this, somewhat tedious, check was implemented, the shifts disappeared as expected. Analogous remarks pertain to angular shifts for a foam in a circular container.

3.3. *Remarks on initial conditions*

The problem of initial states has been considered in the earlier work cited and we may confine our remarks to just a few points. A system with only hexagonal cells is in equilibrium with regard to diffusion, according to von Neumann's law, but it makes an interesting initial condition for deformations, especially in the polydisperse case, when the cells are allowed to have many different areas. This configuration is also useful for diffusion studies, if one creates a few imperfections in an otherwise hexagonal lattice. This can be done by forcing some T1 changes in the hexagonal foam, by 'popping' some sides, or by splitting some cells.

The most useful initial condition for statistical foam studies is the *Voronoi construction* or *Dirichlet tiling* (cf. Grünbaum & Shephard 1987), because it automatically creates a controllable amount of disorder. In the simplest case these cells form a tiling of the plane produced from a number of point 'seeds' that are scattered over the region in question. The cells arise by associating with each seed the set in the plane consisting of points that are closer to it than to any other seed. Each vertex in such a tiling is tri-valent (except for degeneracies due to symmetry). This is probably the most important property with respect to the two-dimensional foam problem. The angles in the Voronoi pattern are, of course, not in general 120°, but we can achieve such angles by allowing the Voronoi tiling to relax elastically.

It is possible to vary the kind of tiling that one obtains by imposing constraints on the distribution of initial seeds. A commonly used device is to impose a 'hard core' on the seeds by requiring any two to be a specified minimum distance apart (see Weaire & Rivier 1984). Voronoi patterns with a hard core tend to have lower values of μ_2 than patterns with no constraint. In some cases it became necessary to create even more regular networks, that could still be considered random. Since the Voronoi construction with the hard-core modification cannot create networks with μ_2 less than about 0.5, we followed Weaire & Lei (1991), and ran the foam 'backwards' for a while (effectively using von Neumann's law with negative κ, but without T2 changes). This could produce values of μ_2 as low as 0.20–0.25.

Another initial condition that we used, for reasons to be described in §5,

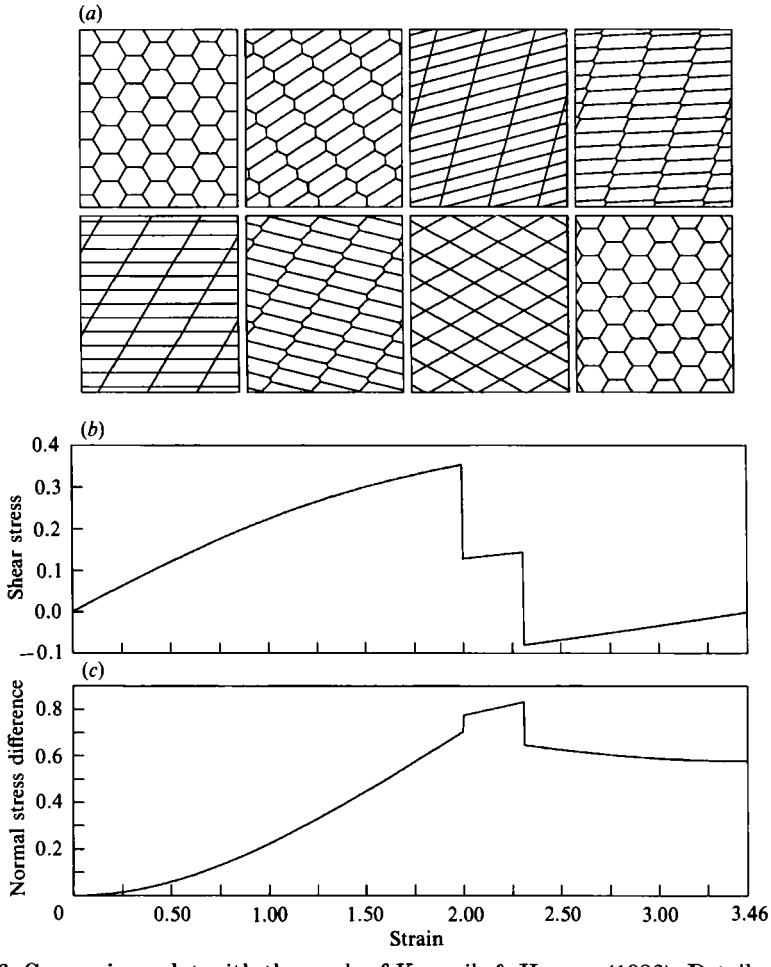

FIGURE 6. Comparison plot with the work of Kraynik & Hansen (1986). Details of the panel by panel comparison are given in the text.

suppressed the number of hexagons. This was accomplished by repeatedly forcing T1 changes for edges between two hexagons, even if they were not particularly short, eliminating two hexagons each time. Clearly not all hexagons will be eliminated by this method, since four cells are affected by every T1 change, and new hexagons may be created as one tries to eliminate others. The method was nevertheless successful in decreasing the initial number of hexagons significantly.

A final useful addition to the roster of initial conditions, suggested to us by A. Kraynik, is to make the foam isotropic, i.e. stress-free. Clearly, regular hexagonal foams are stress-free, but finite, Voronoi-initialized foams, in general, are not (an infinite system would be). The stress in a general initial condition formed from the Voronoi construction may affect the long-time statistics of the foam. To eliminate it, the periodic box containing the foam is simply deformed by an affine transformation, and since the equations are nonlinear, this process can be iterated until the stress-free state is obtained to high accuracy.

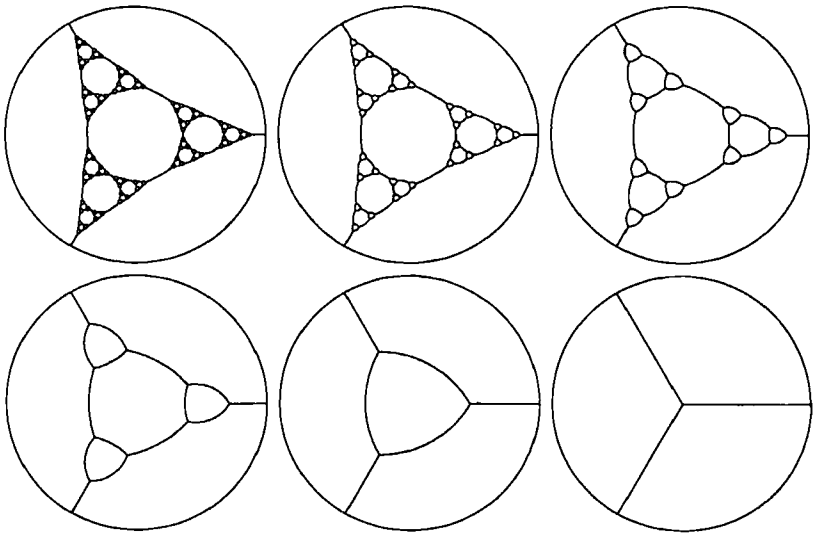

FIGURE 7. Relaxation of a 'fractal foam' decorating a vertex in a system of three larger bubbles in a circle. The case $w = \frac{1}{6}$ with 5 levels (in the terminology of Herdtle & Aref 1991*a*) is shown. The times corresponding to the configuration changes in the various panels are known analytically, and were reproduced by the code to machine precision.

4. Code verification

The first results that we report are designed to verify that the code described in §3 is performing properly. We have explored two principal test cases, which seem to complement one another nicely, and suggest that the code is indeed producing reliable results. The first of these concerns the purely elastic behaviour of a monodisperse-hexagonal foam under shear and extensional deformations investigated by Kraynik & Hansen (1986). For these cases there is no diffusion. Our second test follows the diffusional relaxation of any of a family of 'fractal foams'. We have solved these cases analytically (Herdtle & Aref 1991*a*) and established formulae for the precise times at which different levels in the fractal hierarchy disappear. Several such cases have then been computed using our code, and the times at which reconnections occurred have been recorded. Excellent agreement was obtained in all cases.

Figure 6 shows one result from the simulations aimed at reproducing the results of Kraynik & Hansen (1986). The monodisperse-hexagonal foam is being subjected to an elastic shear deformation. The eight panels in figure 6(*a*) trace the deformations of individual cells in the foam, and should be compared to figure 7 of Kraynik & Hansen (1986). Figures 6(*b*) and 6(*c*) trace the variation of shear stress and normal stress difference with strain and should be compared to figure 6 of Kraynik & Hansen (1986). (We have chosen to connect the curve across the discontinuous jumps corresponding to T1 changes.) Most of the other cases studied by Kraynik & Hansen (1986) were simulated also, and in all cases very good agreement was obtained. The actual times for the reconnections to occur, as well as all the variations in the stress tensor matched the analytical solutions extremely well.

The fractal foam check has already been mentioned in an earlier paper (Herdtle & Aref 1991*a*). An example is shown in figure 7. We are considering a foam situated within a rigid circular boundary. One of the vertices has been 'decorated' by a fractal foam structure. This is characterized by the area ratio, w, between successive levels

in the hierarchy. As shown in Herdtle & Aref (1991*a*) the entire evolutionary process can be calculated in terms of w. In a fractal foam with m levels, the time at which bubbles of level $j = 1, 2, \ldots, m-2, m-1$ disappear is given by

$$t_j = \tfrac{1}{3}w^{j-1}(1-2w). \tag{4.1}$$

(The unit of time here is the area of the fractal foam region divided by the coefficient in von Neumann's law; cf. Herdtle & Aref 1991*a*.) The collapse time for the smallest triangular bubbles, level m, is

$$t_m = \tfrac{1}{3}w^{m-1}. \tag{4.2}$$

We used this analytical solution to check the code for $w = \frac{1}{6}, \frac{1}{8}$, and $\frac{1}{9}$, and up to 6 levels in the fractal hierarchy, and with $w = \frac{1}{5}, \frac{25}{121}$ and up to 4 levels. (Theoretically $0 < w < \frac{1}{3}$. For large w there is a limit to how many levels we can initialize, since the smallest bubbles approach so closely upon elastic relaxation that a T1 change takes place.) Figure 7 illustrates the case $w = \frac{1}{6}$ with 5 initial levels. Both the time for the entire decoration to disappear and all the intermediate times, when different levels in the hierarchy disappear, were found by the code essentially to machine precision.

Two comments may be made. The first is that the collapse of the fractal decoration does not depend on the boundary conditions on bubbles that are not part of the fractal foam itself. This is clear from the analysis, and is here verified numerically. The examples quoted in Herdtle & Aref (1991*a*) used periodic boundary conditions. The second comment is that these solutions give us an explicit instance of an N *vs.* t decay law. Although the bubbles disappear in groups at definite times, it may be useful to consider what power law (if any) describes the disappearance of the various generations of bubbles in a fractal foam with many levels. The number of bubbles present just before time $t = t_j$ is $N_j \approx 3^j/2$. Hence, from $t_j \approx w^j$ we deduce

$$\alpha = -\frac{\log 3}{\log w}. \tag{4.3}$$

This varies from $\alpha = 1.0$ at the theoretical limit $w = \frac{1}{3}$ to arbitrarily small values of α as $w \to 0$ (and corresponds to the virtual origin in time, t_0 in (5.1) below, being equal to 0).

5. Statistical dynamics of large two-dimensional foams

We have conducted a number of numerical experiments on the relaxation of large two-dimensional foams using the code described in the preceding sections. The largest systems that we have explored start with 1024 bubbles, initialized according to one of the recipes described in §3.3. Figure 8 shows six stages in the evolution of such a foam. The panels are drawn for 1024 bubbles (initial condition), 900, 700, 500, 300 and 100. For this particular run (Run II in table 1) the initial state was constructed using the Voronoi procedure with a very mild hard-core constraint. The initial value of μ_2 was relatively large, equal to 1.49. As mentioned, the CPU time required to follow this foam from its start with 1024 bubbles to a final, polydisperse, hexagonal foam, with just a few bubbles within the periodic box is large, and, consequently, the number of different runs that we have performed is rather limited. We collect the ones that we will discuss here in table 1.

The most immediate statistic to monitor is the number of cells, N, as a function of time. Cells are continually disappearing from the foam due to T2 changes. The

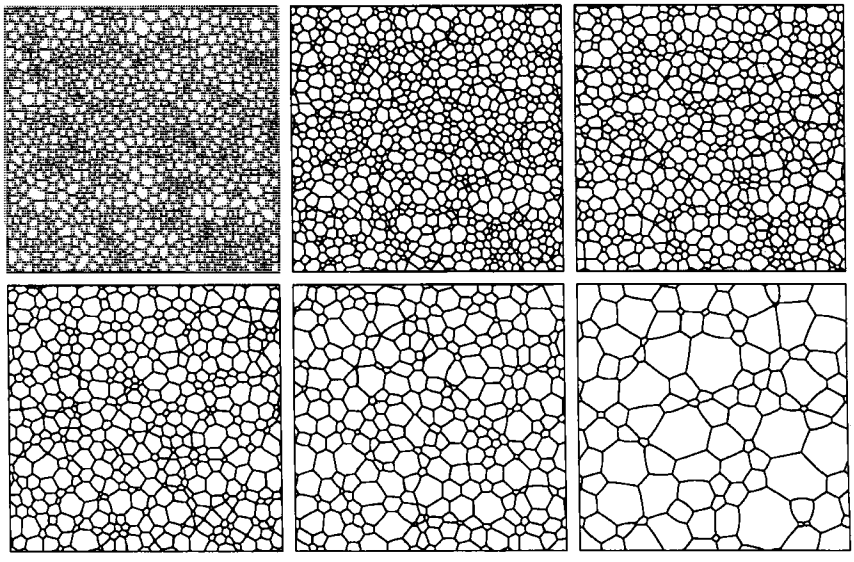

FIGURE 8. Stages in the relaxation of a two-dimensional foam started from 1024 bubbles. Panels are shown for $N = 1024$ bubbles (initial condition, after elastic relaxation), 900, 700, 500, 300 and 100. This is Run II in table 1.

Run	Initialization	Initial bubbles	Initial μ_2
I	Voronoi, no core constraint	1024	1.72
II	Voronoi, very small hard-core constraint	1024	1.49
III	Voronoi, small hard-core constraint	1024	1.17
IV	Voronoi, larger hard-core constraint	1024	0.72
V	Voronoi, no core constraint, hexagons suppressed	1024	1.84
VI	Voronoi, no core constraint, circular boundary	1024	1.53
VII	Voronoi, no core constraint, stress-free initially	1024	1.76
VIII	Voronoi, hard-core constraint, backwards diffusion	512	0.35
IX	Voronoi, hard-core constraint, backwards diffusion	512	0.19
X	Polydisperse hexagonal, line of imperfections	480	0.10
XI	Polydisperse hexagonal, scattered imperfections	480	0.06

TABLE 1. Summary of numerical experiments on large foams

analogy with a two-dimensional turbulent flow may be helpful. If we consider the distribution of bubbles in area and number of sides, the diffusion of gas between bubbles and the T1 changes lead to a 'dual cascade', where bubbles with more than six sides grow, and bubbles with less than six sides contract. Removal from the system occurs for bubbles of three sides, and these bubbles are typically the smallest in size. At the other end of the spectrum, the largest bubbles eventually feel the boundaries of the containing box. The energy of the system resides in the elastic energy of the soap films, and is crudely proportional to N. Thus, we may expect that N will display a power-law dependence on time.

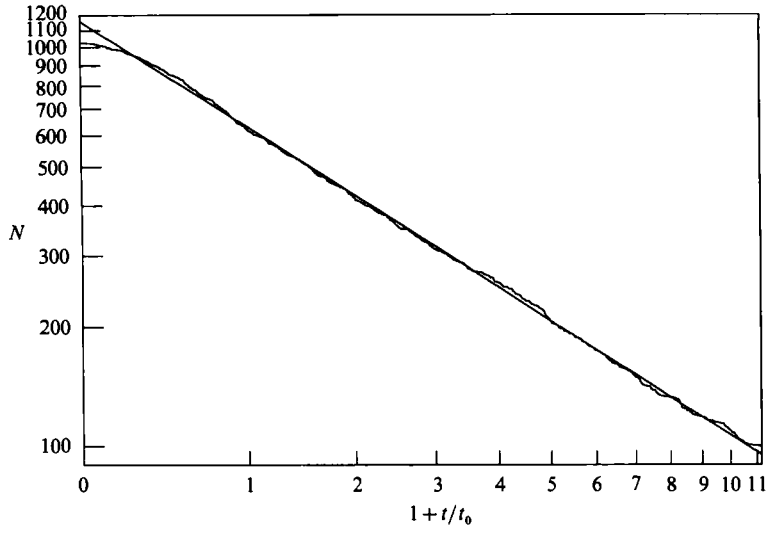

FIGURE 9. Power-law fit, equation (5.1), to the number of bubbles in figure 8 as a function of time (table 1, Run II) for $N = 1024$ to 100 bubbles.

5.1. *Results indicative of a scaling regime*

We found that a three-parameter fit,

$$N = N_0\left(1+\frac{t}{t_0}\right)^{-\alpha}, \tag{5.1}$$

where N_0, t_0 and α are all to be determined in a least-squares sense using $\log N$ and $\log(1+t/t_0)$ as variables, gave very satisfactory representations of the data. An example, from Run II, is shown in figure 9. (We have plotted $\log N$ versus $\log(1+t/t_0)$, although the labels on the abscissa refer to values of t itself.) Equation (5.1) incorporates the idea of a 'virtual origin' in time, when the foam was infinite. In figure 9 (and again in figure 12) the unit of time is taken as the average area per bubble in the initial state divided by the coefficient in von Neumann's law.

Fits to the data of quality similar to that in figure 9 have been found for Runs I–III and VII. Very consistent values of the parameters N_0 and t_0 were found, and values of α in the range 1.13–1.21 were obtained. These are about twice as large as those reported in the experimental literature (Glazier *et al.* 1987). The virtual origin is very important. If one simply measures the slope of a $\log N$ *vs.* $\log t$ plot at some intermediate value of N, say $N = 500$, a slope as shallow as -0.5 may be obtained (leading to a much smaller estimate for α). On the other hand, we have also tried to concentrate our fit on the 'scaling regime', by considering a window, $800 \geqslant N \geqslant 300$, of the data. Here considerable variability of α can result from the choice of window. Stavans (1990) reports $\alpha \approx 1.0$.

The other quantity that has been the subject of considerable attention is μ_2. Both laboratory experiments (Stavans & Glazier 1989) and computations (Weaire & Lei 1990) suggest the existence of a similarity range with $\mu_2 \approx 1.4$. In the laboratory experiments of Stavans & Glazier (1989) two foams, one with air in the bubbles, the other with helium, were followed down to about 100 bubbles. The air foam started with 5000 bubbles, the helium foam with 10000. In the computations of Weaire & Lei (1990) foams of up to 500 bubbles were followed.

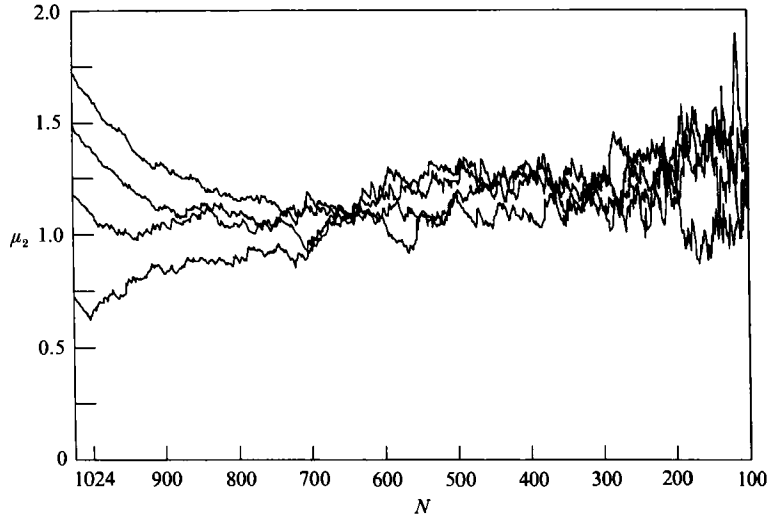

FIGURE 10. Plots of μ_2 as a function of N for Runs I–IV in table 1.

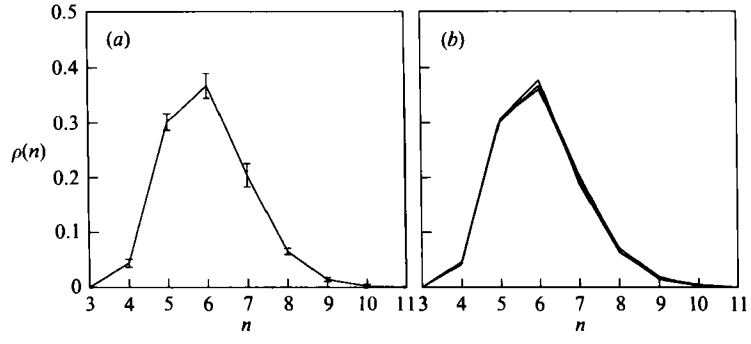

FIGURE 11. (*a*) The number-of-sides distribution, $\rho(n)$, for Run II for $800 \geqslant N \geqslant 200$. The range of variability in $\rho(n)$ is indicated by error bars (standard deviation). (*b*) Comparison of the $\rho(n)$ curve for Runs I–IV showing the degree of scaling.

In figure 10 we plot the history of μ_2 for Runs I–IV from table 1. We find it more satisfactory to plot μ_2 as a function of N rather than time, since the physical time depends on additional factors such as the permeability of the soap films to diffusion of gas. Many more data points are available to us than to the experimenters, since we have the entire foam in digital form at each instant. We note the appearance of a plateau in these curves, after a relatively long, initial transient, with considerable fluctuations. Consistent with the earlier work we do find that a similar plateau is reached regardless of whether the initial μ_2 is higher or lower than the value at the plateau. However, our 'scaling value' of μ_2 is somewhat lower than that reported previously. We find the plateau in μ_2 to occur at 1.2, approximately.

The levelling off of μ_2 suggests that the distribution of the number of sides, $\rho(n)$, is assuming a similarity form. There are two checks to be performed regarding this. On one hand, we want to inquire whether $\rho(n)$ for a given run is assuming a fixed form over some range of N. If this is true, we want to compare the similarity forms of $\rho(n)$ for different runs. Both questions are addressed in figure 11. In figure 11 (*a*) we show $\rho(n)$ for Run II. Using values from $N = 800$–200, the curve connects average values,

and the error bars indicate the standard deviation. Similar scaling is obtained from Runs I, III and IV. In figure 11 (*b*) we have superimposed the average $\rho(n)$ for Runs I–IV, again using data from $N = 800$–200 bubbles, showing the level of scaling between runs. Clearly, a strong case for a similarity form of $\rho(n)$ emerges in this diagram.

It is particularly noteworthy that our similarity form for $\rho(n)$ has $\rho(6) > \rho(5)$. This is as one would expect, since hexagonal cells are in local equilibrium in the diffusive dynamics of von Neumann's law. However, the similarity form given by Stavans & Glazier (1989), albeit obtained only for a few hundred bubbles, clearly has $\rho(5) > \rho(6)$. This difference is also consistent with the higher scaling value of μ_2 reported by these authors. Weaire & Lei (1990) do not show a scaling form for $\rho(n)$.

We have counted the number of cells that are hexagons with three or more hexagons as neighbours. Normalized by the total number of cells, this proportional measure of 'order' is found to converge during the scaling state to a value of 0.15 ± 0.03 (averaged over Runs I–IV).

We have also monitored the ratio of T1 and T2 changes, and found it to asymptote to 3:2. A rough understanding of this may be obtained as follows. Consider some of the more common combinations of neighbouring cells, such as a quadrilateral and a hexagon, or two pentagons. In the former case a T1 change can produce a three-sided and a five-sided cell. The first of these disappears in a T2 change. The second undergoes two T1 changes and a T2 before it disappears. In total, three T1 and two T2 changes are required as this pair disappears from the foam. This is precisely the 3:2 ratio observed. Similarly, the two pentagons require three T1 changes to produce, sequentially, two four-sided and then two three-sided cells, which vanish in two T2 changes. Again a ratio of 3:2 emerges. This is not always the case. For example, a pentagon and a hexagon require four T1 and two T2 changes to disappear, and a pentagon and a quadrilateral require two T1 and two T2. Taken together these processes, thus, require six T1 and four T2 changes, again yielding the ratio 3:2.

An interesting question is whether a disordered system of cells has an elastic energy (proportional to the total length of soap films) that is higher or lower than an equivalent system of hexagons with the same total area and number of cells (A. Kraynik, personal communication). The value of the energy for the equivalent system of hexagons is $E_{\mathrm{hex}} = (2\sqrt{3}NA_{\mathrm{tot}})^{\frac{1}{2}}$. It is well known that the energy of a polydisperse-hexagonal system does not change when the sizes of the cells are changed in such a manner that the total area remains constant. It is possible to come up with examples of disordered foams where the energy is higher than E_{hex} (make one T1 change in a regular hexagonal foam; one finds numerically that the energy can increase with fixed N), and examples where it is lower than E_{hex} (add small three-sided cells at the vertices of the hexagonal foam; N can be increased arbitrarily at essentially no increase in total film length). These possibilities led us monitor the ratio of energy of our evolving, disordered foam to E_{hex}. An elastically relaxed foam started from unconstrained Voronoi polygons has a value of the scaled energy, E/E_{hex}, in the range 0.95–0.99, whereas a foam generated by using the hard-core Voronoi initialization has a higher value of E/E_{hex} in the range 0.99–1.05.

The remarkable – and somewhat surprising – conclusion from our simulations is that in the scaling regime, foams seem to assume a constant value of $E/E_{\mathrm{hex}} = 0.945 \pm 0.010$. Thus, the energy of the evolving, disordered foam is always slightly less than that of the corresponding hexagonal foam. It is tempting to conjecture that a similar result would hold in three dimensions for the energy of an evolving foam

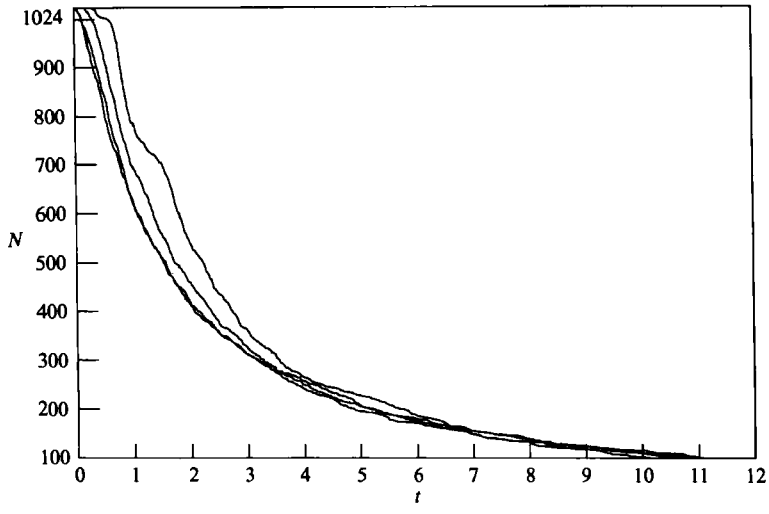

FIGURE 12. The number of cells versus time (the unit of which is total area of the foam scaled by the coefficient in von Neumann's law) for Run IV ('top' curve) showing the 'waves' of T2 changes. For comparison N versus t is also plotted for Runs I–III. (Run II is the case fitted to a power law in figure 9.)

relative to the energy of an equivalent system of Kelvin tetrakaidecahedra. We do not understand the dynamic origin of this result, but it is reminiscent of notions of 'marginal stability' or 'self-organized criticality' that have been advanced for the evolution of similar statistical systems.

5.2. *Challenges to scaling*

So far, we have concentrated on those results of our simulations that appear to verify the notion of a scaling regime, albeit with governing statistical quantities that are quite different from what has been reported previously in the literature. We now turn to issues that indicate exceptions to the scaling picture, or – maybe more accurately – the limitations to observing scaling behaviour inherent in working with systems as small as 1000 bubbles. After performing a few simulations it is readily apparent that obtaining a scaling regime is extremely sensitive to specifics of the initial condition, and the time to reach the scaling state can vary widely from run to run.

When the larger hard-core constraint is applied to the Voronoi initial condition, an interesting phenomenon occurred that was not seen in the unconstrained Voronoi cases. Initially very few T2 changes occur in the system. Then, suddenly, many occur almost simultaneously. Then again there is a period where few occur; then again many. After a couple of these 'waves' no more are really discernible. Figure 12 shows a plot of N versus t for Run IV (the 'top' curve of the set), and, for comparison, the N versus t plot for Runs I–III. (Run II was fitted to the power law, (5.1), in figure 9; the scaling of the time in figure 12 is the same as used in figure 9.) The reason for these waves is that in the hard-core Voronoi initial condition most of the bubble areas are nearly equal, and there are very few three- or four-sided cells. As the diffusion starts, all the five-sided cells have their areas reduced at the same rate (by von Neumann's law). Then, as they become small, T1 and T2 changes occur, and many cells disappear at nearly the same time. The same process then repeats itself with a new set of five-sided cells. The number of waves visible in the N *vs.* t plot (figure 12) clearly depends on the initial area distribution. Typically, after two or three

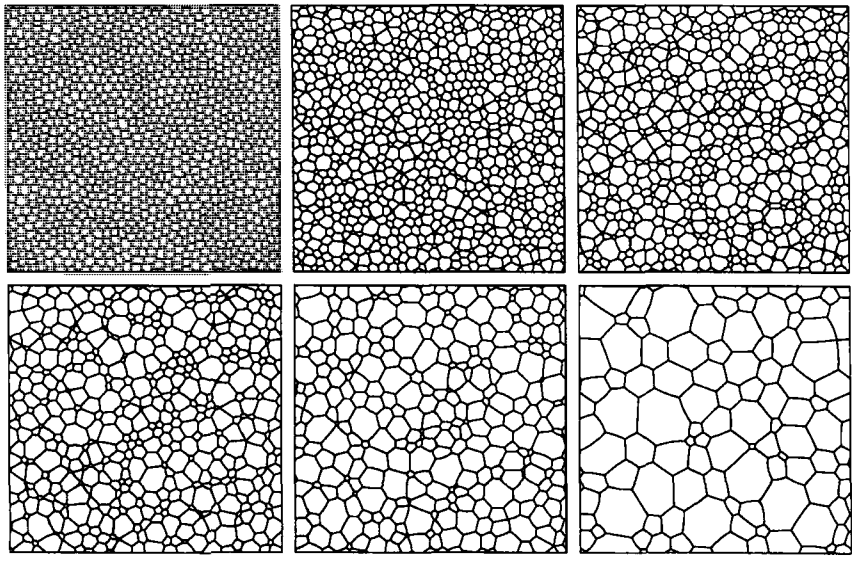

FIGURE 13. Stages in the relaxation of a more 'ordered' two-dimensional foam. Panels are shown for $N = 1024$ bubbles (initial condition), 900, 700, 500, 300 and 100. This is Run IV in table 1. This illustration should be compared to figure 8. While there are qualitative differences between the two runs in the first three panels, the last three appear statistically similar.

waves the area distribution has become broad enough for this phenomenon to end. Also, clearly, a power-law fit for N *vs.* t, as in (5.1), will not succeed very well. Additionally, this 'ringing' will appear in some other statistics, although neither the μ_2 *vs.* N scaling (figure 10) nor the scaling of $\rho(n)$ (figure 11) are particularly affected. Figure 13 shows stages in the evolution of the initially 'ordered' foam, Run IV, for comparison with figure 8.

The earlier laboratory and computational work showed one interesting effect associated with initial conditions. This is the apparently steep rise in μ_2 with time when the initial condition is highly ordered. To explore this phenomenon we initialized smaller systems (512 bubbles; Runs VIII and IX in table 1) with low initial μ_2. This configuration was created by running a hard-core Voronoi foam (with $\mu_2 \approx 0.5$) backwards for some time (see §3.3), a procedure that could reduce μ_2 to about 0.2 due to T1 changes. After the T1 changes have occurred, the foam is no longer reversible; thus, when it is run forward in time again, the network does not just backtrack the construction of the initial condition.

We expected that the low initial value would always cause an overshoot of μ_2 before it relaxed to its scaling value, as observed by Weaire & Lei (1990) and, particularly, by Stavans & Glazier (1989). Indeed, as the initial $\mu_2 \to 0$, a singularity must exist in the system, since for $\mu_2 = 0$ we have a polydisperse-hexagonal foam, which will not evolve at all under diffusion. When plotted versus N, we found initial transients for μ_2 that were far less dramatic than plots of μ_2 *vs.* t in the earlier work would suggest. Moreover, we found that μ_2 can either have an overshoot, or it can go smoothly to the plateau value without overshoot. Interestingly, the run with the smaller initial μ_2 (Run IX) showed an essentially monotonic approach to an asymptotic value.

For a polydisperse-hexagonal foam μ_2, of course, vanishes. Very small values of μ_2 can thus be obtained by effecting a few T1 changes in such a foam, and using the

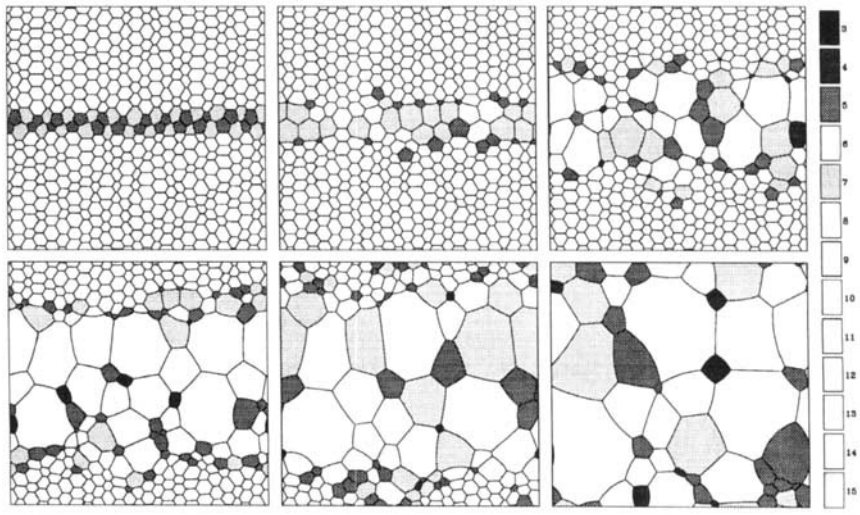

FIGURE 14. Evolution of an initially polydisperse-hexagonal foam with a line of 'imperfections' due to T1 changes (Run X). Panels shown are for $N = 480$, 450, 350, 250, 150 and 45 bubbles. Bubbles are shaded according to their number of sides, as indicated by the bar at the right.

resulting, elastically relaxed state as the initial condition. Runs X and XI were of this kind. In Run XI we had a few scattered 'imperfections' (the T1 changes will produce pairs of five-sided and seven-sided cells). In Run X a line of such imperfections was initialized, resembling the 'grain boundaries' seen experimentally in bubble rafts of essentially identical, hexagonal cells (Glazier *et al.* 1987; the classical bubble raft experiments of Bragg & Nye (1947) contain much more fluid, and the dry foam limit is not applicable). Figure 14 shows stages in the evolution of Run X. The gradual widening of the 'grain boundary' is very similar to what is observed experimentally. For this run μ_2 did, indeed, grow to very large values. In the final panel of figure 14, μ_2 has reached its maximum of 3.24.

The observation of long-lived transients and the apparent influence of initial conditions raises the question of whether the predominance of hexagons in the scaling regime discussed is anything but a remnant from the initial condition, where hexagons typically are the most numerous type of cell. In order to address this question we conducted a simulation (Run V in table 1) where the number of hexagons in the initial state was considerably reduced (cf. §3.3). In the initial states used for Runs I–IV, $\rho(6) \approx 0.3$–0.5 and $\rho(6)/\rho(5) \approx 1.1$–$1.8$. In Run V we had $\rho(6) \approx 0.15$, and $\rho(6)/\rho(5) \approx 0.36$. Nevertheless, as the foam evolved, a $\rho(n)$ distribution was eventually reached, at $N \approx 500$, which is close to the scaling form of figure 11, and definitely has $\rho(6) > \rho(5)$. The scaling value of $\rho(6)$, figure 11(*b*), is 0.35, approximately, and for this scaling distribution $\rho(6)/\rho(5) \approx 1.2$.

A related concern is the influence of stresses along the boundaries of the periodic box. In separate calculations with a smaller number of cells we found that a sheared foam (without diffusion) would rearrange to produce a $\rho(n)$ distribution that was strongly peaked at $n = 6$ and very symmetric about its peak (i.e. $\rho(6-k) \approx \rho(6+k)$ for $k = 1$, 2, 3, and insignificant numbers of cells with 10 sides or more). The small boundary stress in the simulations reported so far thus might be biasing the $\rho(n)$ distribution. This would not remove the inconsistencies with earlier work, since in the computations of Weaire & Lei (1990) no attempt was made to remove stresses either.

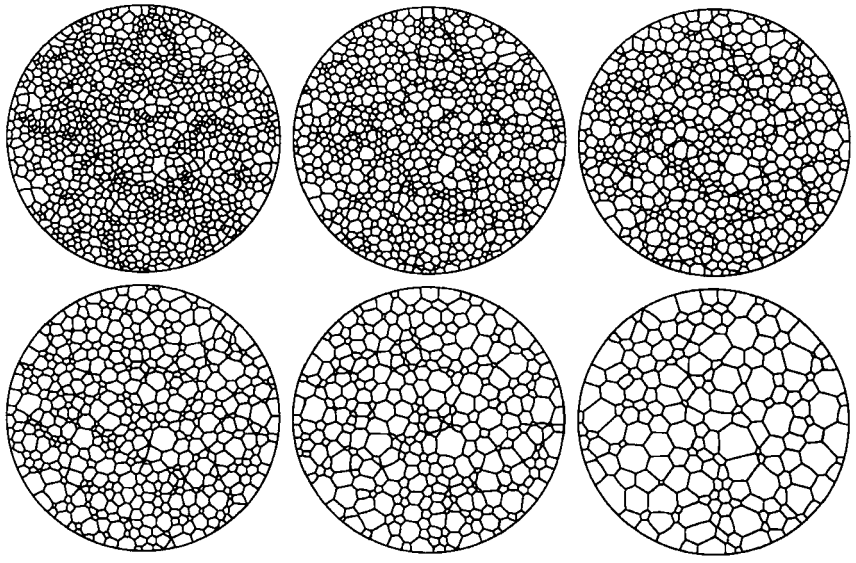

FIGURE 15. Evolution of a large foam in a circular boundary, Run VI. Panels shown are for $N = 1024$ (initial condition), 900, 725, 550, 375 and 200 bubbles.

We have performed one large run with initially stress-free boundaries (see §3.3) and standard Voronoi initialization (Run VII). Fortunately, the results from this run are indistinguishable from those of Runs I–IV.

In a similar vein, but aimed primarily at the possible effects of lateral boundaries in laboratory experiments, we performed a large run for a foam contained within a circular boundary (Run VI). For this the Voronoi construction had to be reformulated to accommodate the boundary. Statistics, taken over internal cells only, again show no appreciable deviation from the results reported for Runs I–IV. Stages from this calculation are shown in figure 15. Along the boundary we see a preponderance of five-sided cells, but it appears that within very few cell layers the presence of the rigid boundary 'heals', and we return to a state that is statistically indistinguishable from the doubly periodic foam.

5.3. *Additional statistical measures*

Ever since Lewis (1928) noted that the areas of cells on the skin of a cucumber were on average proportional to their number of sides,

$$\langle A_n \rangle = \lambda(n - n_A), \tag{5.2}$$

this same law has been sought in other cellular systems, such as foams and metal grains. It is found to hold in many instances. However, there are frequently deviations for few- and many-sided cells (but the statistics on such cells is also usually poor, since there tend to be few of them).

Another, similar law claims that the average perimeter of a cell is proportional to its number of sides:

$$\langle P_n \rangle = A(n - n_P). \tag{5.3}$$

This is frequently mentioned in connection with metal grains. The literature seems to discuss both laws in relation to foam networks, and it is not clear which should really apply. One can attempt to argue the perimeter law, (5.3), on the basis of equipartition of energy, proportional to film length, between the films of the foam.

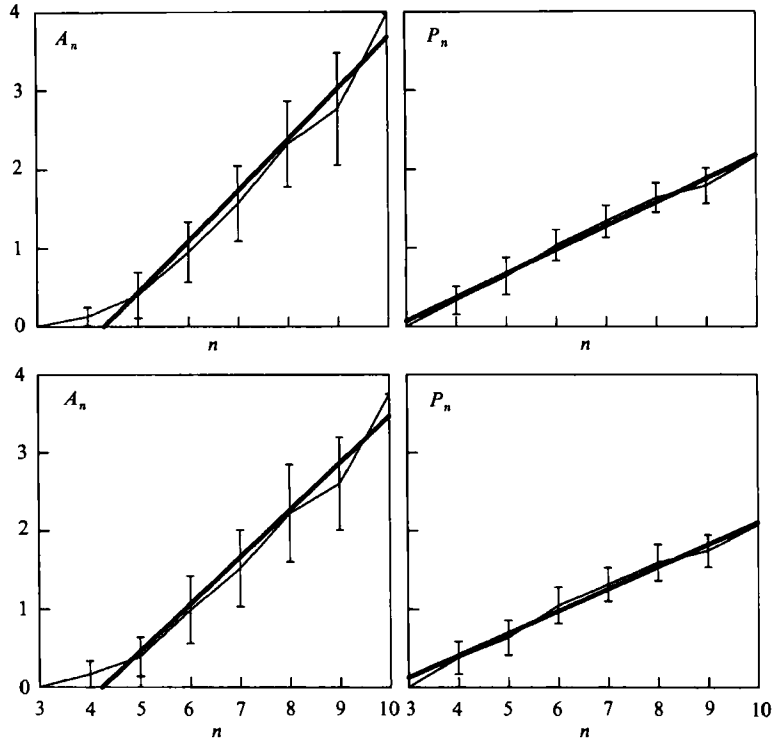

FIGURE 16. Check of Lewis' law, (5.2) left column, and the perimeter law, (5.3), right column, for Run II with $N = 800$ and 500. The polygon line connects averages for each $n = 3, \ldots, 10$, the error bars show the standard deviation. The straight solid line is a least-squares fit. The scaling of the ordinates is described in the text.

Then an n-sided bubble should, indeed, have n 'units' of energy, or film length. However, such a requirement is much stronger than the scaling being claimed, since it implies that all side lengths should be roughly equal, and this does not appear to be the case. Rivier has argued that Lewis' law plays the role of an 'equation of state' in a statistical mechanics treatment of a cellular aggregate (see his review, Rivier 1990, where many further references may be found).

In the present simulations we have checked both laws. Figure 16 shows data from Run II at $N = 800$ and $N = 500$ for each. Both Lewis' law and the perimeter law have been tested. The polygon line in each panel of figure 16 connects averages for each $n = 3, \ldots, 10$, and the error bars indicate the standard deviation. The areas plotted along the ordinate in figure 16 have been scaled by the average area per bubble, i.e. by the total foam area divided by N. The perimeters have been scaled by the 'average perimeter', i.e. by twice the total edge length divided by N. From such data a straight line fit can be obtained using the method of least squares, and from this one gets the slopes, λ and A, and the intercepts, n_A and n_P, in (5.2) and (5.3). For our simulations the perimeter law (5.3) provides a slightly better fit than Lewis' law (5.2), particularly for bubbles with a small number of sides.

In figure 17 (a, b) we show the time evolution of the slope A and the intercept n_P as the foam evolves for runs I–III. During periods of evolution where there are no reconnections the slope should increase linearly with time, and the intercept decrease inversely with time. However, the frequent reconnections that occur in the evolving foam lead to near constancy of both A and n_P as shown in figure 17 over an extended

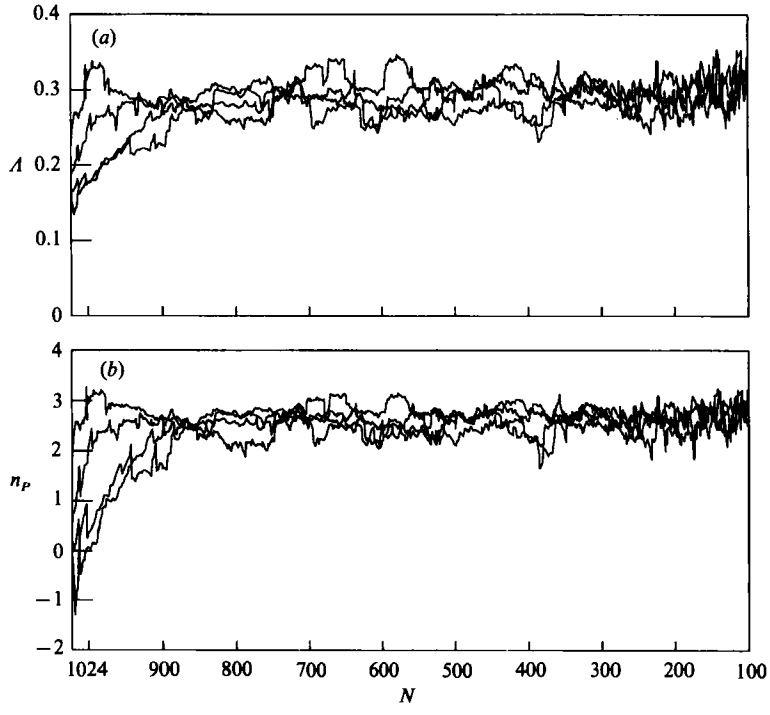

FIGURE 17. Variation with N of (*a*) the coefficient A, and (*b*) intercept n_P, in the perimeter law, (5.2).

range of N, which overlaps the scaling regime discussed previously. Rivier (1990) presents theoretical arguments in favour of this behaviour. In the scaling regime the slope, A, settles down to 0.3, approximately. The intercept grows from a rather small value initially to about 2.5. These results appear to be new, and give the parameters in the perimeter law (and in Lewis' law) an interesting dynamical significance.

Similar remarks apply to the so-called Aboav–Weaire law (Aboav 1970, 1980; Weaire 1974), which states that the average number of sides of cells that are neighbours to n-sided cells, ν_n, should vary as

$$\nu_n = a + \ell n^{-1} \tag{5.4}$$

(cf. Aref & Herdtle 1990). At any instant during foam evolution this law is followed quite closely. It is again interesting to view (5.4) from a dynamical point of view, and track the variation of the coefficient a with time by fitting the form (5.4) to the data from the simulation at each instant. (The coefficient ℓ is given in terms of a and μ_2; see Aref & Herdtle 1990.) Fluctuations of about 10% in a are found, with a mean value of 4.8, approximately. There is, however, no indication of a more constant value of a within the scaling regime itself, as there is for other statistical quantities. Thus, verification of the Weaire–Aboav law did not appear as a good diagnostic of scaling behaviour.

6. Discussion, conclusions and extensions

The most significant result of the simulations reported here is that the properties of the scaling regime in a two-dimensional dry foam, as it coarsens due to gaseous diffusion, appear to depend on long-range couplings within the foam. These are

captured by the present computer code, but may not have been well represented in earlier simulation work. The long-range impact of T1 changes in the foam becomes vividly obvious when the simulations are turned into a video animation. Then one sees, unequivocally, that T1 reconnections have a finite range effect that extends over several layers of neighbouring bubbles. When a T1 change occurs, a shifting of bubbles several 'sites' away is clearly evident.

The differences between the laboratory experiments of Glazier *et al.* (1987) and the present simulations can have any of several explanations. The experiments are conducted with a finite amount of fluid trapped within the films of the foam. Hence, as the foam coarsens, more and more fluid must accumulate in Plateau borders. Further, there are effects due to drainage onto, and wetting of, the parallel plates confining the foam. Finally, as the films thicken, the dynamics of surfactants on the films will change, leading to possible changes in both surface tension and the rate of gaseous diffusion through soap films. Any one of these effects could make the experimental and the simulation results deviate from one another. It is possible that the recently proposed use of Langmuir monolayers to study two-dimensional foam dynamics (cf. Knobler 1990; Berge, Simon & Libchaber 1990; Lucassen, Akamatsu & Rondelez 1991), and techniques such as the one applied by Stavans (1990) to remove fluid from the films during the coarsening, can go some way towards bringing simulations and experiments into closer agreement.

The approach of adding Plateau borders to the analytic/computational model is also very worthwhile, but much work remains to be done. The fluid in the entire system of films can be viewed as one multiply-connected 'bubble' of a second phase. A single pressure is associated with this 'bubble'. It has a very large number of sides, all of which are circular arcs, if we ignore flow of liquid within the films. The Young–Laplace law then applies to determine the radii of these circular arcs as before. The main problem is the generalization of von Neumann's law, which assumes a uniform rate of gas transport across the film. This is unlikely to be true if there are substantial variations in the thicknesses of individual films. In the limit of a small but finite liquid content, the liquid may be assumed localized at the vertices of the dry foam 'skeleton' of the structure. These pockets of liquid are the Plateau borders. Three circular arcs delimit each one, meeting two and two in cusps. In this case we would add to our vector $\boldsymbol{X}$ in (2.4) a single pressure for the fluid component, and, in place of the V vertex coordinates of the dry foam, introduce $3V$ coordinates corresponding to the three meeting points of the bounding films of the Plateau borders for each vertex. The angle conditions on these films are that they meet two and two at 0°. They meet with the films that connect Plateau borders to each other at angles of 180°. This can clearly be substituted into the formalism in §2, in place of the 120° conditions, without too much trouble. The fluxes across interfaces must now be computed individually, and von Neumann's law does not apply, in general. The procedures outlined in §2 then go through as before. However, the modelling of topology changes requires additional considerations. Furthermore, very small time steps will always be required. Bolton & Weaire (1991) have attempted to capture some of all this by a simple 'decoration' procedure of the vertices of a dry foam.

The close agreement between the results for the scaling regime seen in the laboratory experiments of Glazier *et al.* (1987), and the numerics of Weaire & Lei (1990) is to a large extent fortuitous, in our view. We have outlined computational issues that cloud the numerical results, and it is not clear that the experiments provide a good realization of the 'canonical' model of a dry foam. For both *a priori* and *a posteriori* reasons we believe that treating the entire coupled foam at each step

of a numerical simulation is absolutely essential. The general idea of a scaling regime, as displayed in figures 9, 10 and, particularly, figure 11 seems verified. However, the role of long-lived transients and the necessity of working with large systems must be constantly kept in mind.

We mention that it is possible to generalize the canonical dry foam model to include a compressible dispersed phase, in particular a gas obeying the ideal gas law. This arises by substituting for the vector $\boldsymbol{Y}$ in (2.5) another vector

$$\tilde{\boldsymbol{Y}} = (M_1, \ldots, M_F, \Theta_1, \Phi_1, \ldots, \Theta_V, \Phi_V), \tag{6.1}$$

where $M_1, \ldots, M_F$ are the masses of the air in the individual bubbles. Fluxes of mass across interfaces are now tracked in place of fluxes of area. Such a generalization to compressible dispersed phase has been implemented, but the results for diffusive relaxation did not appear particularly interesting. However, the resulting elastic equilibria, as the surface tension is gradually increased for a fixed mass distribution of the dispersed phase, produce intriguing results on bubble differentiation, that will be reported separately.

We thank A. Kraynik, K. Mysels, C. Pozrikidis, D. Reinelt, R. Skalak, C. M. Surko, and N. Rivier for comments, discussion and criticism. We thank D. Weaire for his comments, and for sending us several preprints from his research group. We are indebted to R. Leary of the San Diego Supercomputer Center (SDSC) for discussions on linear algebra software, which led to substantial improvements in the efficiency of our code.

This work was supported by National Science Foundation PYI award CTS 84-51107. T.H. also acknowledges fellowship support from Office of Naval Research. Computing resources at SDSC have been invaluable. SDSC is supported by NSF.

REFERENCES

ABOAV, D. A. 1970 The arrangement of grains in a polycrystal. *Metallography* **3**, 383–390.

ABOAV, D. A. 1980 The arrangement of cells in a net. *Metallography* **13**, 43–58.

AREF, H. & HERDTLE, T. 1990 Fluid networks. In *Topological Fluid Mechanics* (ed. H. K. Moffatt & A. Tsinober), pp. 745–764. Cambridge University Press.

BEENAKKER, C. W. J. 1988 Numerical simulation of a coarsening two-dimensional network. *Phys. Rev.* A**37**, 1697–1702.

BERGE, B., SIMON, A. J. & LIBCHABER, A. 1990 Dynamics of gas bubbles in monolayers. *Phys. Rev.* A**41**, 6893–6900.

BOLTON, F. & WEAIRE, D. 1991 The effects of Plateau borders in the two-dimensional soap froth. I. Decoration lemma and diffusion theorem. *Phil. Mag.* B**63**, 795–809.

BRAGG, L. & NYE, J. F. 1947 A dynamical model of a crystal structure. *Proc. R. Soc. Lond.* A**190**, 474–481.

GEORGE, A. & NG, E. 1984 SPARSPAK: Waterloo Sparse Matrix Package. *Dept. Computer Science, Univ. Waterloo, Res. Rep.* CS-84-37, 47 pp.

GLAZIER, J. A. 1989 Dynamics of cellular patterns. Ph.D. thesis, University of Chicago.

GLAZIER, J. A., GROSS, S. P. & STAVANS, J. 1987 Dynamics of two-dimensional soap froths. *Phys. Rev.* A**36**, 306–312.

GLAZIER, J. A. & STAVANS, J. 1989 Nonideal effects in the two-dimensional soap froth. *Phys. Rev.* A**40**, 7398–7401.

GRÜNBAUM, B. & SHEPHARD, G. C. 1987 *Tilings and Patterns*. W. H. Freeman.

HERDTLE, T. & AREF, H. 1989 Numerical simulation of two-dimensional foam. *Bull. Am. Phys. Soc.* **34**, 2296 (abstract only).

HERDTLE, T. & AREF, H. 1991*a* Relaxation of fractal foam. *Phil. Mag. Lett.* **64**, 335–340.

HERDTLE, T. & AREF, H. 1991*b* On the geometry of composite bubbles. *Proc. Roy. Soc. Lond.* A**434**, 441–447.

ISENBERG, C. 1978 *The Science of Soap Films and Soap Bubbles.* Somerset: Woodspring Press.

KERMODE, J. P. & WEAIRE, D. 1990 2D-FROTH: A program for the investigation of 2-dimensional froths. *Comput. Phys. Commun.* **60**, 75–109 (referred to herein as KW).

KNOBLER, C. M. 1990 Seeing phenomena in Flatland: Studies of monolayers by fluorescence microscopy. *Sci.* **249**, 870–874.

KRAYNIK, A. M. & HANSEN, M. G. 1986 Foam and emulsion rheology: A quasistatic model for large deformations of spatially-periodic cells. *J. Rheol.* **30**, 409–439.

LEWIS, F. T. 1928 The correlation between cell division and the shapes and sizes of prismatic cells in the epidermis of *Cucumis. Anat. Rec.* **38**, 341–376.

LUCASSEN, J., AKAMATSU, S. & RONDELEZ, F. 1991 Formation, evolution and rheology of two-dimensional foams in spread monolayers at the air–water interface. *J. Colloid Interface Sci.* **144**, 434–448.

MADDOX, J. 1989 Soap bubbles make serious physics. *Nature* **338**, 293.

NEUMANN VON, J. 1952 Discussion remark concerning paper of C. S. Smith, 'Grain shapes and other metallurgical applications of topology'. In *Metal Interfaces*, pp. 108–110. Am. Soc. for Metals, Cleveland, Ohio.

PLATEAU, J. A. F. 1873 *Statique Experiméntale et Théorique des Liquides Soumis aux Seules Forces Moléculaires.* Gauthier-Villars.

PRINCEN, H. M. & MASON, S. G. 1965 The permeability of soap films to gases. *J. Colloid Sci.* **20**, 353–375.

RIVIER, N. 1990 Geometry of random packings and froths. In *Physics of Granular Media* (ed. D. Bideau & J. Dodds) Nova Science.

STAVANS, J. 1990 Temporal evolution of two-dimensional drained soap froths. *Phys. Rev.* A**42**, 5049–5051.

STAVANS, J. & GLAZIER, J. A. 1989 Soap froth revisited: dynamic scaling in the two-dimensional froth. *Phys. Rev. Lett.* **62**, 1318–1321.

SULLIVAN, J. M. 1991 Generating and rendering four-dimensional polytopes. *Mathematica J.* **1** (3), 76.

WEAIRE, D. 1974 Some remarks on the arrangement of grains in a polycrystal. *Metallography* **7**, 157–160.

WEAIRE, D. & KERMODE, J. P. 1983*a* The evolution of the structure of a two-dimensional soap froth. *Phil. Mag.* B**47**, L29–L31.

WEAIRE, D. & KERMODE, J. P. 1983*b* Computer simulation of two-dimensional soap froth I. Method and motivation. *Phil. Mag.* B**48**, 245–259.

WEAIRE, D. & KERMODE, J. P. 1984 Computer simulation of two-dimensional soap froth II. Analysis of results. *Phil. Mag.* B**50**, 379–395.

WEAIRE, D., KERMODE, J. P. & WEJCHERT, J. 1986 On the distribution of cell areas in a Voronoi network. *Phil. Mag.* B**53**, L101–L105.

WEAIRE, D. & LEI, H. 1990 A note on the statistics of the mature two-dimensional soap froth. *Phil. Mag. Lett.* **62**, 427–430.

WEAIRE, D. & RIVIER, N. 1984 Soap, cells and statistics – Random patterns in two dimensions. *Contemp. Phys.* **25**, 59–99.

WEJCHERT, J., WEAIRE, D. & KERMODE, J. P. 1986 Monte Carlo simulation of the evolution of a two-dimensional soap froth. *Phil. Mag.* B**53**, 15–24.